



**HAL**  
open science

## **Anisothermal behaviour of unirradiated CWSR zircaloy-4 fuel clads under RIA conditions**

Ahmed Chaieb, N. Mozzani, A. Parrot, A. Ambard, Alain Köster, Jérôme  
Crépin

► **To cite this version:**

Ahmed Chaieb, N. Mozzani, A. Parrot, A. Ambard, Alain Köster, et al.. Anisothermal behaviour of unirradiated CWSR zircaloy-4 fuel clads under RIA conditions. Top Fuel 2018, Sep 2018, Prague, Czech Republic. 12 p. hal-01917119

**HAL Id: hal-01917119**

**<https://minesparis-psl.hal.science/hal-01917119>**

Submitted on 9 Nov 2018

**HAL** is a multi-disciplinary open access archive for the deposit and dissemination of scientific research documents, whether they are published or not. The documents may come from teaching and research institutions in France or abroad, or from public or private research centers.

L'archive ouverte pluridisciplinaire **HAL**, est destinée au dépôt et à la diffusion de documents scientifiques de niveau recherche, publiés ou non, émanant des établissements d'enseignement et de recherche français ou étrangers, des laboratoires publics ou privés.

# ANISOTHERMAL BEHAVIOUR OF UNIRRADIATED CWSR ZIRCALOY-4 FUEL CLADS UNDER RIA CONDITIONS

**A. CHAIEB, N. MOZZANI, A. PARROT, A. AMBARD**

*Département Matériaux et Mécanique des Composants  
EDF, Electricité de France, Avenue des Renardières, Ecuelles 77818, Moret-sur-Loing Cedex, France*

**A. KÖSTER, J. CREPIN**

*Centre des Matériaux - Mines ParisTech CNRS UMR 7633  
63 - 65 rue Henry Desbrières, BP 87, F-91003 Evry cedex, France*

## ABSTRACT

This paper presents new experimental thermo-mechanical tests recently developed in order to understand the behaviour of fuel clads under anisothermal conditions. The experimental setups permitted material testing in complex conditions representative of real RIA loading (high strain and heating rates) coupling simultaneous mechanical and thermal loading. Mechanical properties are studied and compared to isothermal ones. Results showed a clear history effect at low strain rates, this effect seems to disappear at high strain rates due to rapid mechanical loading which limits heating before failure. 2D and 3D FEM are illustrated with applied thermo-mechanical loadings. These numerical simulations allowed us to evaluate the history effect during anisothermal tensile tests using a constitutive law identified on isothermal uniaxial tests.

## 1. Introduction

RIA (Reactivity Initiated Accident) is an accidental scenario considered in Pressurized Water Reactors safety analysis. It is characterised by fast and complex thermo-mechanical transients affecting the fuel rod clads and could potentially lead to their failure.

Tests performed in experimental reactors CABRI [1], [2], [3] and NSRR [4], [5] permitted to define these transients: high strain rates (up to  $5 \text{ s}^{-1}$ ), high heating rates (up to  $1000 \text{ °C.s}^{-1}$ ) and variable biaxial load path.

The purpose of this study is to understand the behaviour of unirradiated cold-work stress-relieved Zircaloy-4 during these transients from newly developed tests. From this viewpoint, efforts have been carried out to set up uniaxial and biaxial anisothermal tensile tests providing loading conditions quite similar to RIA transients.

The Prometra database [6] and many other experimental studies [7], [8], [9], [10], [11] have identified the role of many factors involved in RIA transients such as temperature, oxidation, hydriding, strain rate, biaxiality and irradiation under isothermal loading conditions. These results allow us to compare anisothermal and isothermal mechanical properties.

Uniaxial anisothermal tensile tests have been developed and carried out at two strain rates ( $5 \cdot 10^{-1}$  and  $5 \text{ s}^{-1}$ ) and several heating rates in the range  $85\text{-}560 \text{ °C.s}^{-1}$  in order to check the relative importance of heat-up versus mechanical loading. They are described in the first part of the paper.

The second part of the paper is dedicated to the recently developed biaxial anisothermal test carried out with controlled displacements in order to obtain strain ratios near to the equal-biaxial case.

Finally, FEM simulations taking into account the real experimental conditions are presented. For that purpose, a constitutive behaviour law identified on isothermal tests has been used to evaluate the history effect.

## 2. Uniaxial anisothermal tensile tests

### 2.1 Specimen and testing conditions

To understand the effect of anisothermal loading on the material behaviour during uniaxial tensile tests, a Gleeble® testing device has been modified to perform rapid tests.

The apparatus is equipped with a 50 kN load cell specifically calibrated before tests in the range of interest. The material is heated by electric current using the Joule effect. The heating is controlled by an Eurotherm® regulator Model 2604 connected to WinATS® 6.0 software. A specific holding grips system is designed and installed on the apparatus platform to maintain tubular specimens of 70 mm length. The heated length is 10 mm.

The tube clad has been tested only along the axial (rolling) direction at constant displacement rates. All experiments are performed on fresh non-hydrated CWSR Zircaloy-4 tubes commonly used in PWRs French reactors.

As shown in Fig 1, full-field strains are provided by a 3D stereo digital image correlation (DIC) thanks to an applied painting (white and black speckling pattern). Temperature field is measured by an infrared thermo-graphic camera. In addition, a type K thermocouple is welded in the middle of the tube specimen to monitor the test and calibrate the thermo-graphic camera.

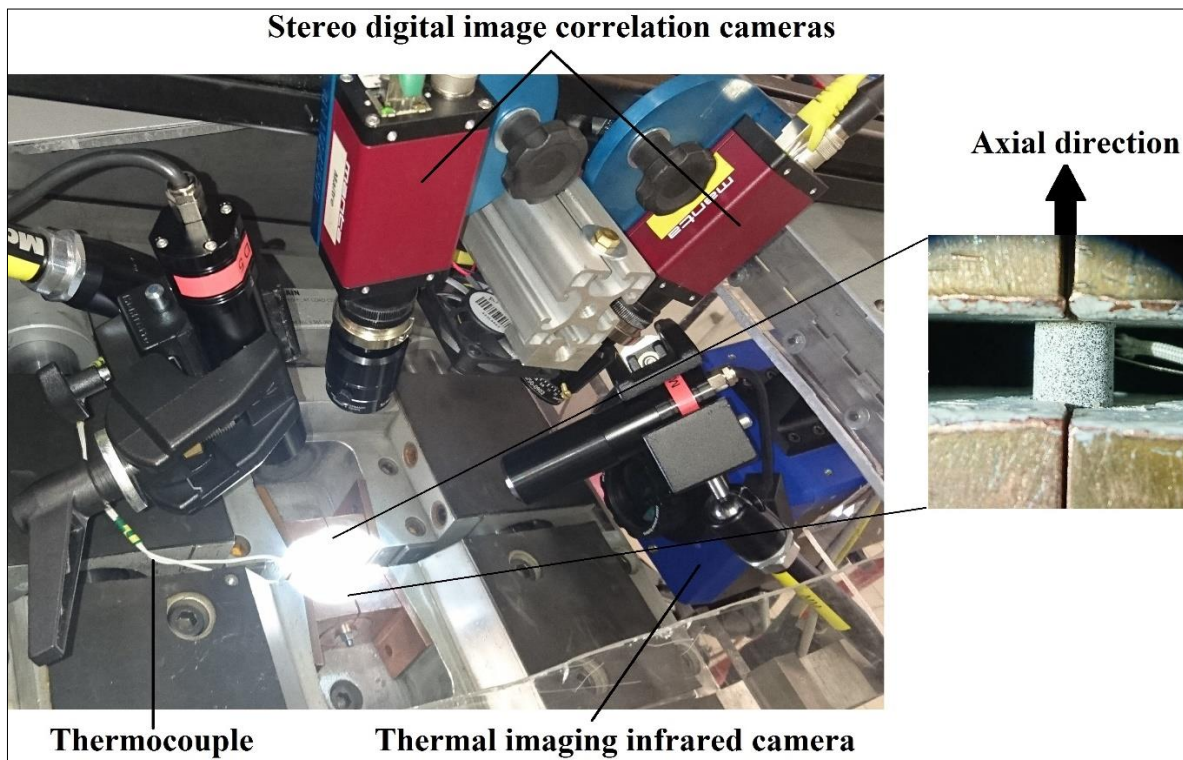


Fig 1. Instruments used for the axial anisothermal test

The apparatus and both cameras store data at the same frequency.

As a first step, the thermal gradient was checked using field measurements. A typical axial temperature gradient of 8°C is measured on 2 mm length as shown in Fig 2. It is judged acceptable for all tests. Strains are then calculated with an initial gauge length of 2 mm.

The thermal gradient presented above is recorded at the point of maximum stress.

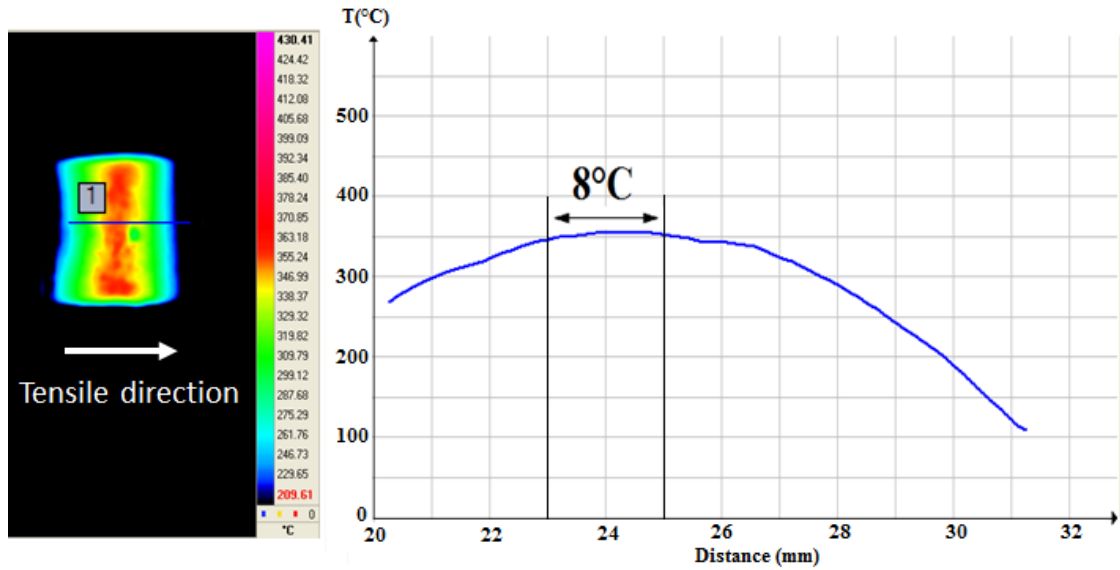


Fig 2. Thermal axial gradient measured during a  $\dot{T} = 353 \text{ }^\circ\text{C} \cdot \text{s}^{-1}$   $\dot{\epsilon} = 5 \text{ s}^{-1}$  test

Concerning the heating sequence, the material is rapidly heated up to 280°C, close to the in-service temperature. This temperature is stabilized for 1 min and followed by a heating ramp at the desired rate. A typical heating sequence is presented in Fig 3. The mechanical loading is triggered when the measured temperature increases linearly with time.

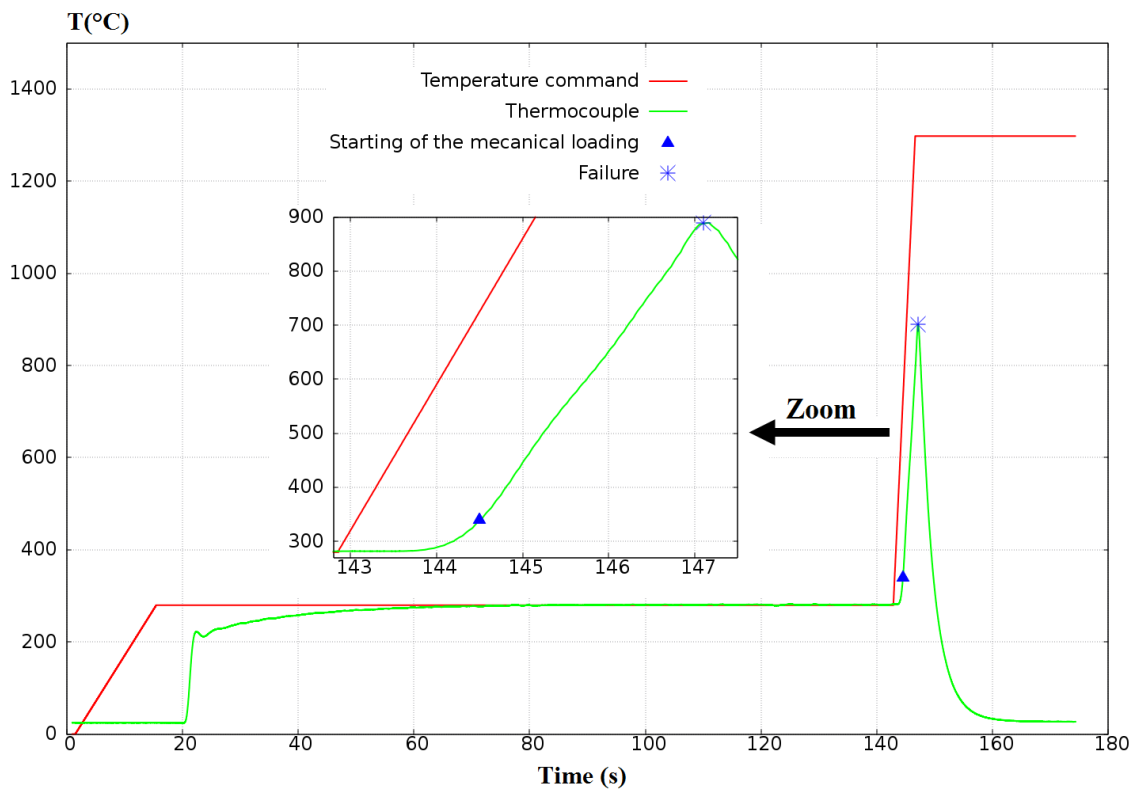


Fig 3. A typical sequence of thermal loading

The test matrix, detailed in Tab 1, is composed of two strain rates and several heating rates in the range of 85-560°C.s<sup>-1</sup>. The initial temperature at which the mechanical loading is triggered is also mentioned for each test.

$\dot{\epsilon}$ (s <sup>-1</sup> )	$\dot{T}$ (°C.s <sup>-1</sup> )	Initial temperature (°C)
0.5	117	363
0.5	208	408
0.5	245	376
0.5	256	358
0.5	316	448
0.5	395	501
0.5	396	472
0.5	400	469
5	85	321
5	231	366
5	353	383
5	558	409

Tab 1. Test conditions of anisothermal tensile tests

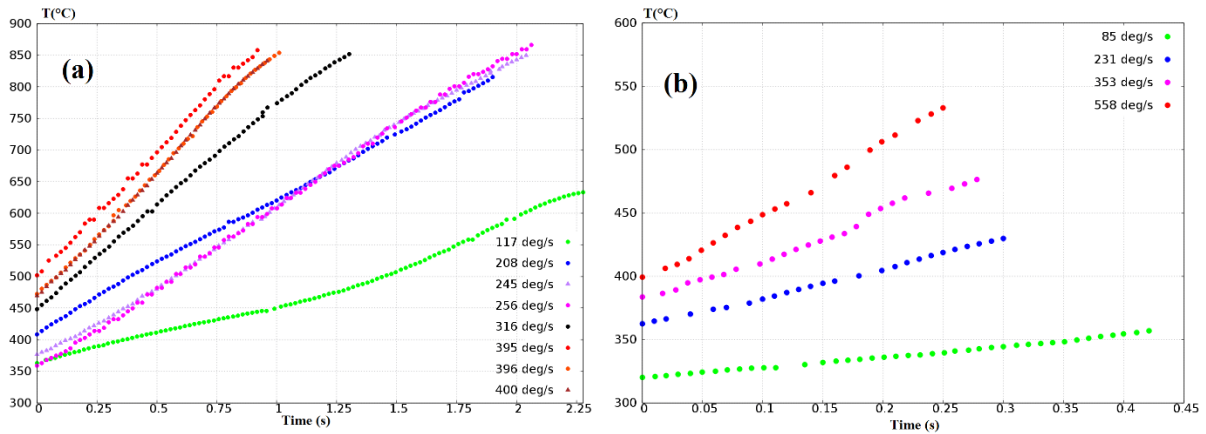


Fig 4. Temperature ramps applied during (a)  $\dot{\epsilon} = 5 \cdot 10^{-1} \text{ s}^{-1}$  and (b)  $\dot{\epsilon} = 5 \text{ s}^{-1}$  tests

Fig.4 shows the temperature ramps applied during the test at the two investigated strain rates. The maximal failure temperatures are 1020°C and 532°C for slow and rapid tests respectively. At high strain rates, temperatures remain lower than 532°C because the tests are very short (around 300 ms). The mechanical transients are so fast that the material had not enough time to be heated at high temperature; it fails before.

## 2.2 Experimental results and discussion

In this part, we describe the effect of the heating rate on the material behaviour. The tensile curves of tests carried at  $5 \cdot 10^{-1} \text{ s}^{-1}$  and  $5 \text{ s}^{-1}$  are plotted in Fig 5 and Fig 9 respectively. Nominal stress is plotted versus the local average strain measured inside the region of interest (2 mm of length) where the temperature is assumed to be homogenous. Points at specimen failure are estimated by extrapolating the strain versus displacement correlations.

The flow stress decreases with temperature increase. The maximal temperature increase during the tests reaches  $\Delta T = 552^\circ\text{C}$  (test performed at  $5 \cdot 10^{-1} \text{ s}^{-1}$  and  $316^\circ\text{C} \cdot \text{s}^{-1}$ ).

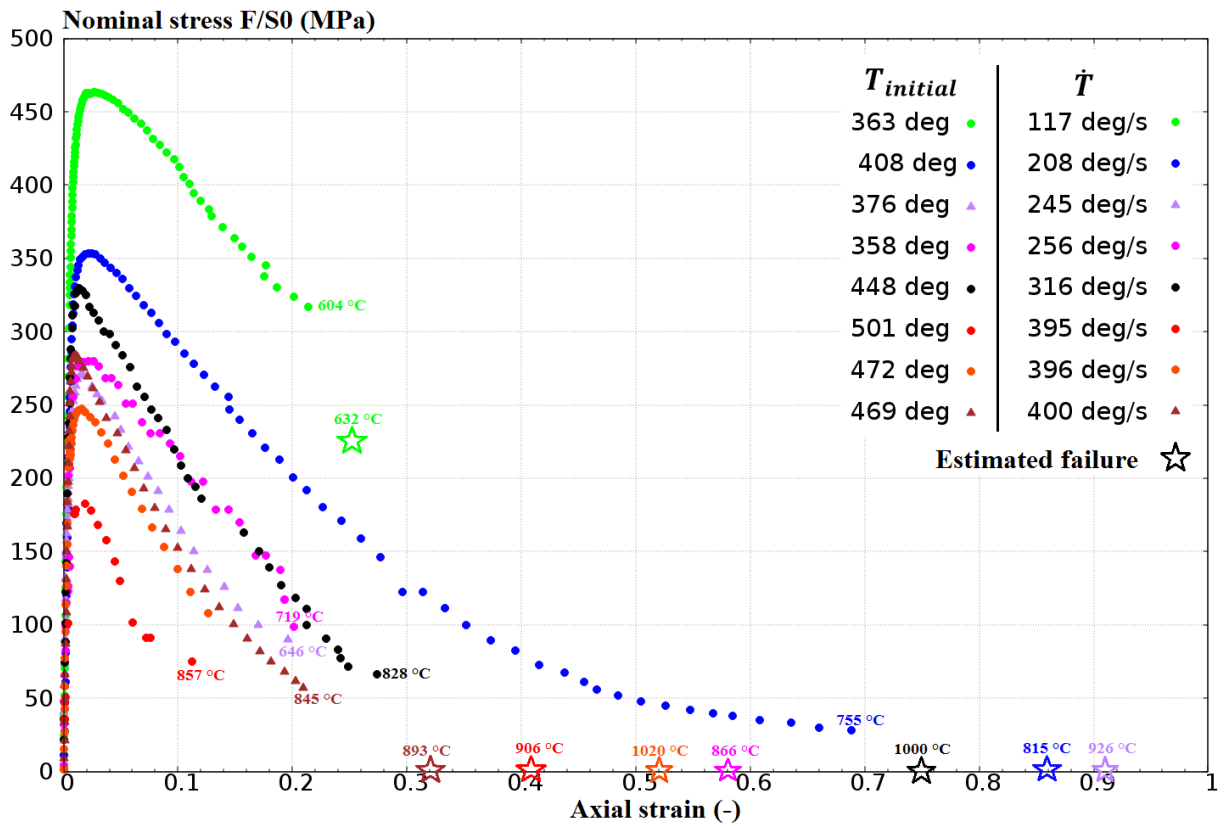


Fig 5. Anisothermal tensile curves at  $\dot{\epsilon} = 5.10^{-1} s^{-1}$

An important area reduction due to temperature increase during the test is observed in Fig 6 (a). Striction increases with failure temperature.

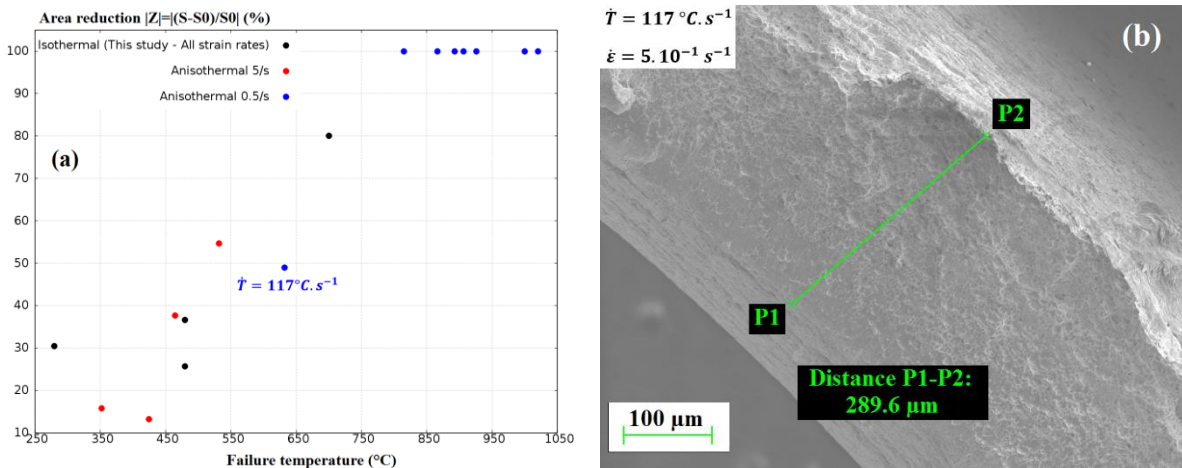


Fig 6. Area reduction as a function of failure temperature (a) Failure surface of the test carried out at  $\dot{T} = 117^{\circ}C.s^{-1}$   $\dot{\epsilon} = 5.10^{-1} s^{-1}$  (b)

At a strain rate of  $5.10^{-1} s^{-1}$ , the test carried out at  $117^{\circ}C.s^{-1}$  put aside, the flow stress decreases progressively during deformation until reaching a zero value. As shown in Fig 6, the reduction of area is about 50% for the test carried out at  $117^{\circ}C.s^{-1}$  and is 100% for all other slow tests, no fracture surface is observable. This viscous behaviour is systematically observed when the temperature exceeds  $650^{\circ}C$ . On the contrary, failure is always obtained at non-zero stresses for all rapid tests. When the failure occurs at non-zero stresses, the analysis of fracture surfaces of the specimens shows a ductile failure of the material regardless of heating and

strain rates.

Rapid ( $5 \text{ s}^{-1}$ ) anisothermal tests exhibit the behaviour expected from the isothermal tests. In Fig 7 the ultimate nominal stress is plotted as function of temperature. For anisothermal tests, data plotted correspond to the nominal stress recorded at the point of maximal load associated with the temperature measured at this point. In fact, this apparent maximal stress results from a competition between two phenomena: the increase of stress due to hardening and the decrease of stress due to temperature increase. Even if it is not an ultimate stress per se, it is nevertheless a lower bound estimate of the ultimate stress at the measured temperature.

Fig 7 shows that anisothermal ultimate stress is similar to that obtained under isothermal conditions at high strain rates.

Some isothermal tests carried out on our experimental facility agree well with the Prometra [6] isothermal database, thus confirming that flow stress differences could not be attributed to differences of test setup.

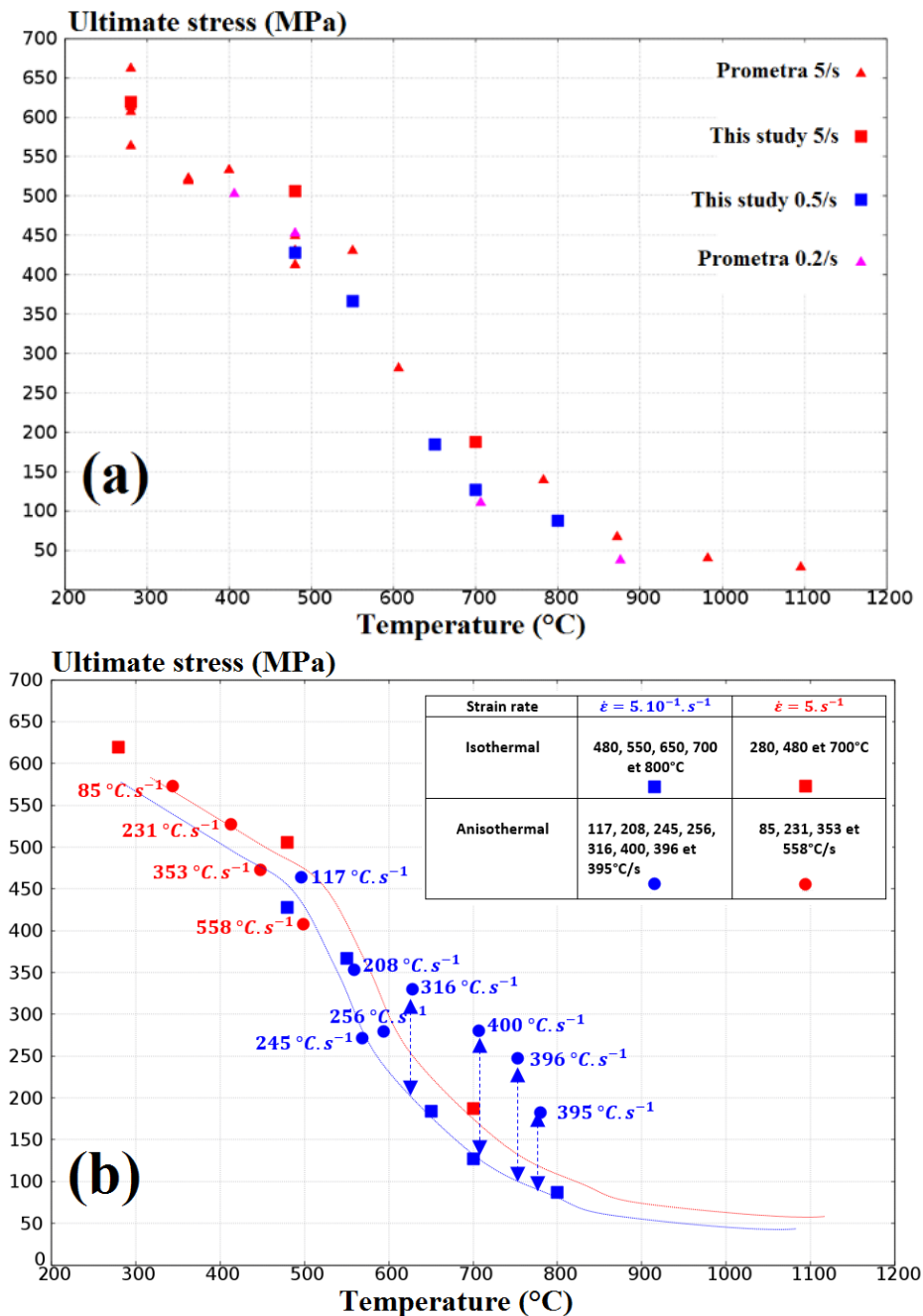


Fig 7. Isothermal ultimate stress (a) Anisothermal Vs isothermal ultimate stress (b)

The history of the thermo-mechanical loading seems to have no effect during rapid tests. However, for slower tests, the anisothermal ultimate stress is higher than the isothermal one and the effect of anisothermal loading becomes important, especially at elevated heating rates. In other words, at a given temperature during the anisothermal tests, the flow stress is higher than the flow stress measured during isothermal tests at the same temperature, for the same strain.

An effect of the loading history on the material behaviour is clearly highlighted. If we refer to the temperature recorded at the point of anisothermal ultimate stress, the ultimate stress of an isothermal test carried at the same temperature is lower than the ultimate stress of the anisothermal test. That is not observed for rapid tests since the too short loading duration is masking this effect. Rapid tests do not involve enough temperature evolution to decrease the flow stress.

Ultimate stress deviation observed during slow tests at high heating rates could be explained by material annealing or recrystallization. According to Hunt studies [12], a delay in the recrystallization process occur during thermal transients. Generally, under isothermal conditions, recrystallization starts at 580°C and is complete at about 680°C, a range where we start to find deviations from isothermal cases.

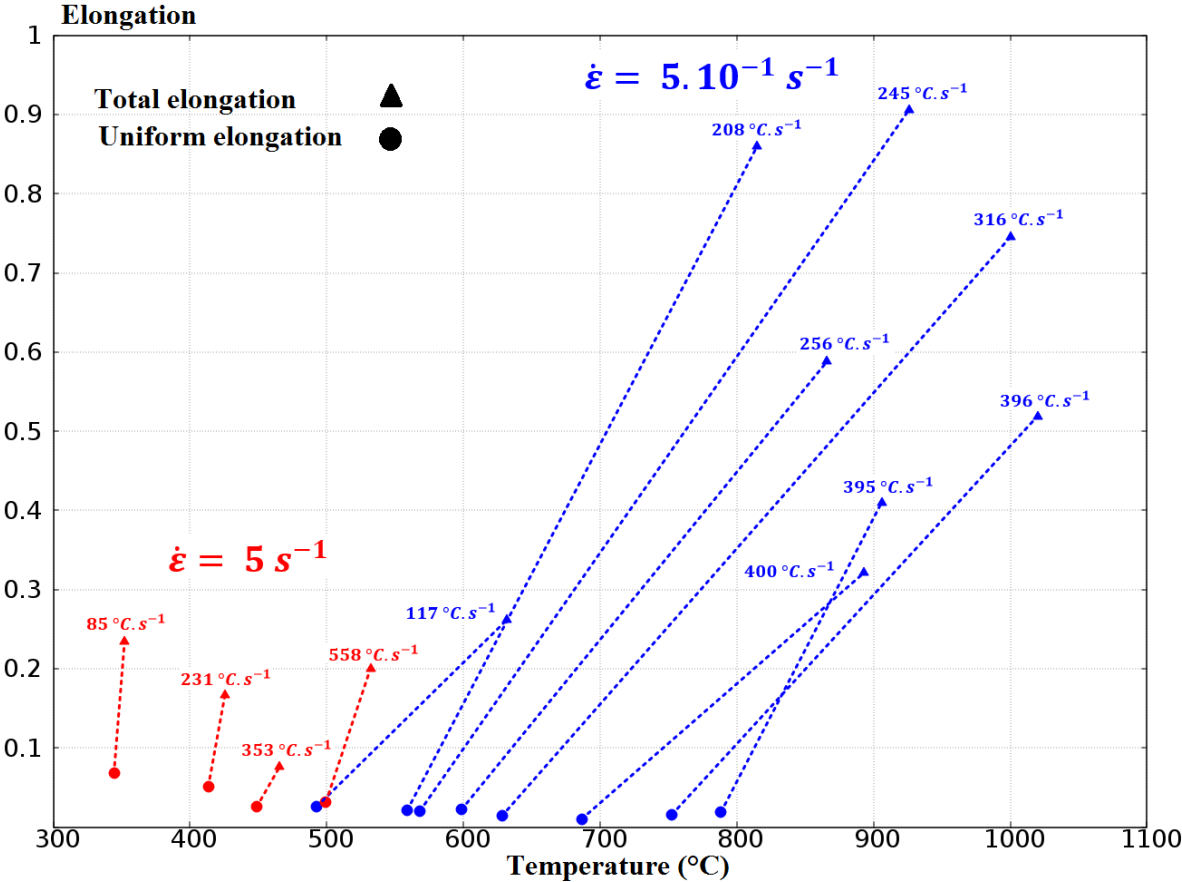


Fig 8. Uniform and total anisothermal elongations as a function of temperature

Fig 8 shows the evolution of uniform and total elongations as a function of temperature recorded at the points of maximum stress and failure, respectively.

The evolution of the uniform elongation is similar to the isothermal case obtained in Prometra [6] program. Total elongations are estimated from strain-displacement curves. For slow tests, total elongation increases considerably when temperature exceeds 650°C. In the range 820-1100°C, total elongation seems to decrease with heating rate (so temperature) increase which may be associated with the phase transformation phenomenon. In fact, burst tests show a similar minimum of ductility in the 800 to 900°C temperature range [13].

## 2.3 FEM

In this part, we try to assess the history effect thanks to a constitutive behaviour law identified on isothermal Prometra [6] tensile tests carried at several temperatures and strain rates.

It is a visco-plastic law taking into account the effect of temperature, irradiation and anisotropy. It does not include a damaging model nor the thermal expansion of the material. So far, only rapid tests are simulated because they are more representative of real RIA conditions.

Fig 9 presents the results of the numerical 2D simulations in the r-z plane using Code\_Aster® (www.code-aster.org) and Salome\_Meca (www.salome-platform.org). It is an axi-symmetric calculation where we model the real clad geometry (a thickness of 0.57 mm and a length of 2 mm).

Experimental temperatures from the thermocouple are applied homogeneously throughout the specimen. Displacements from the DIC measurements are applied at the boundaries.

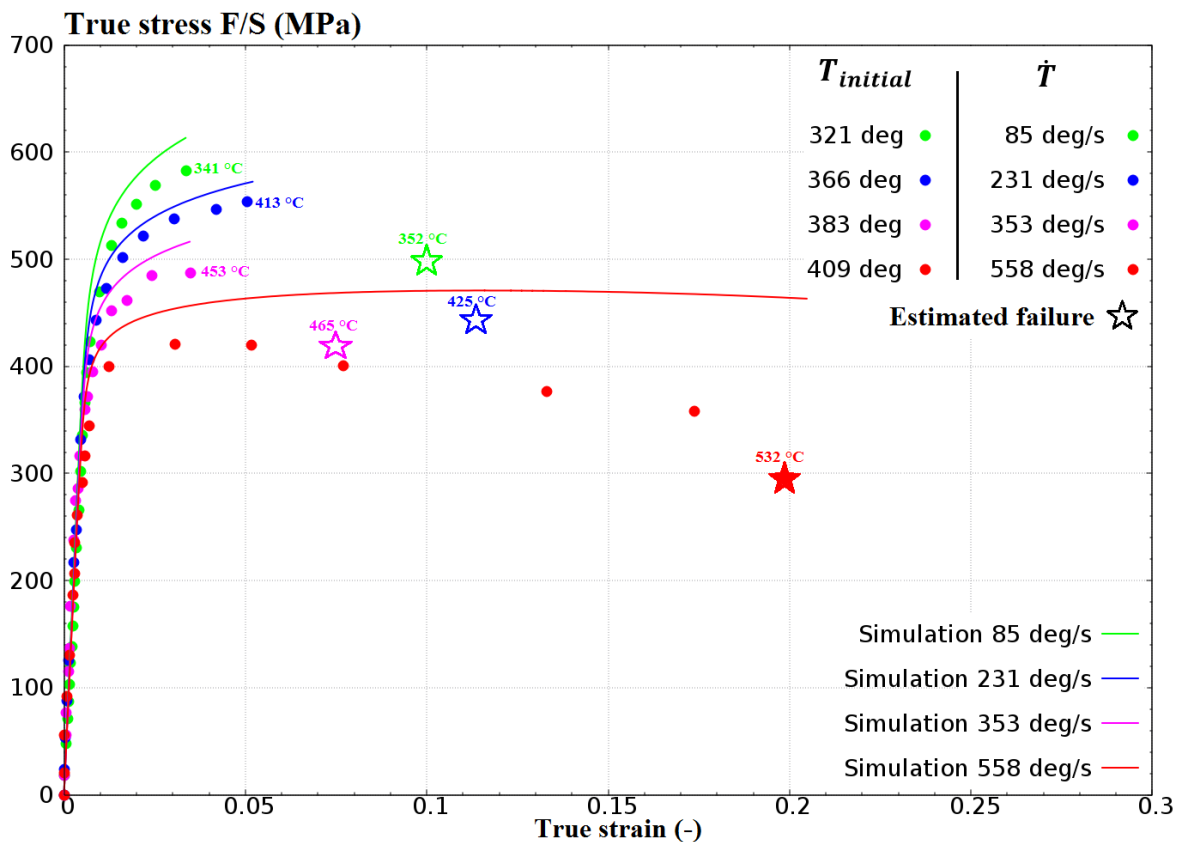


Fig 9. Experimental Vs Simulated tensile curves carried at  $5 \text{ s}^{-1}$

The constitutive behaviour law reproduces well the clad behaviour during anisothermal tensile rapid tests. In the range of 300-550°C, at  $5 \text{ s}^{-1}$  the history effect seems to be low.

The next step of the work will be the simulation of the slower tests.

## 3. Biaxial anisothermal tensile tests

The second part of this work consisted in the development of a testing device dedicated to the study of biaxial and anisothermal loading of a CWSR Zircaloy-4 thin sheet.

### 3.1 Specimen and testing conditions

An Instron® 8800 model biaxial coplanar apparatus equipped with 4 crossing heads (2 axis) is used to test 0.8 mm thick sheets. Specimen thickness is reduced to 0.4 mm in the central

area to force strain localisation. A customized induction coil (Fig 10) is designed and connected to an induction furnace. The same heating sequence, as previously described in Fig 3, is applied. The furnace was connected to the apparatus software for synchronization reasons. The device is equipped with the same field measurements capability as for uniaxial tests. One K-type thermocouple is also welded on the backside of the specimen at 3 mm from the specimen centrum for furnace regulation. The first test carried at  $144^{\circ}\text{C}\cdot\text{s}^{-1}$  under conditions near to equal-biaxial strain is presented in the next section.

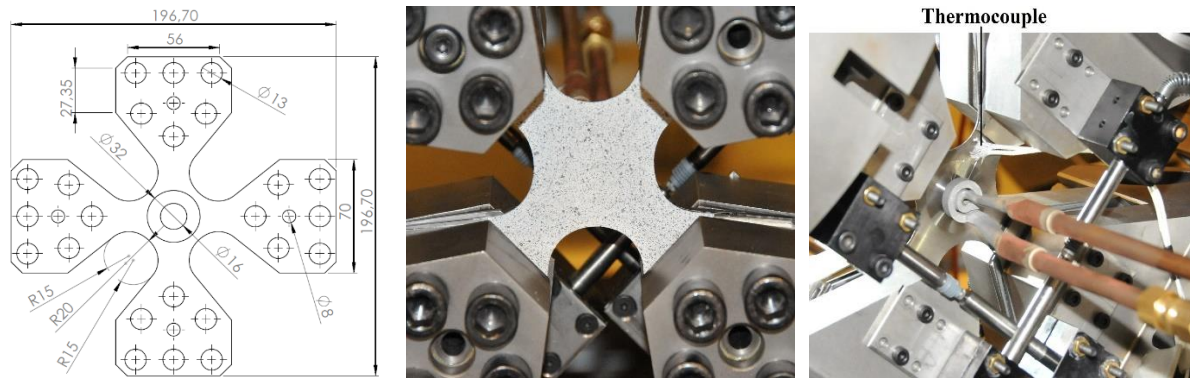


Fig 10. Specimen geometry and induction coil for biaxial anisothermal test

### 3.2 Experimental results and discussion

The test is carried out at  $144^{\circ}\text{C}\cdot\text{s}^{-1}$ . Machine displacements are controlled thanks to sensors installed on the specimen gripping system. The displacement rate is  $4\text{ mm}\cdot\text{s}^{-1}$  for both axes which correspond to the rolling and transverse directions of the specimen. Failure occurs in the zone where maximal temperatures and strains are recorded with field measurements. This test lasts 670 ms, Fig 11 shows strain and temperature fields recorded at 560 ms. Due to the induction coil's geometry, temperature could be higher in the rolling direction (horizontal direction in Fig 11-(a)).

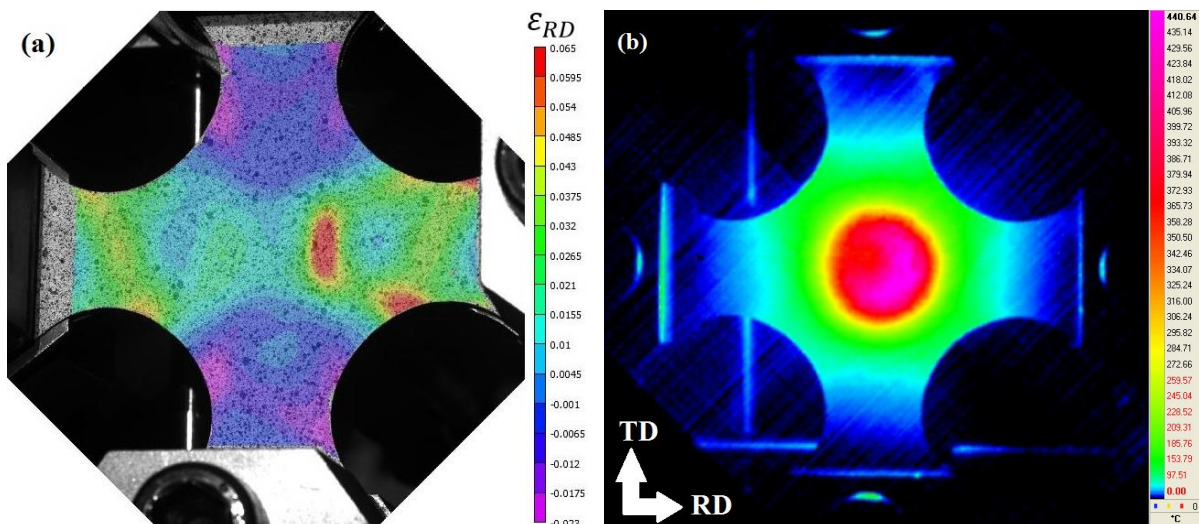


Fig 11. Strain field component along the rolling (horizontal) direction (a) and Temperature field ( $^{\circ}\text{C}$ ) (b) at 560 ms

Strains and strengths are measured in both directions and plotted as function of time and strains respectively in Fig 12. Due to complex specimen geometry, FEM is necessary to calculate stress fields. Initial and failure temperatures measured at the thermocouple are  $381^{\circ}\text{C}$  and  $483^{\circ}\text{C}$  respectively.

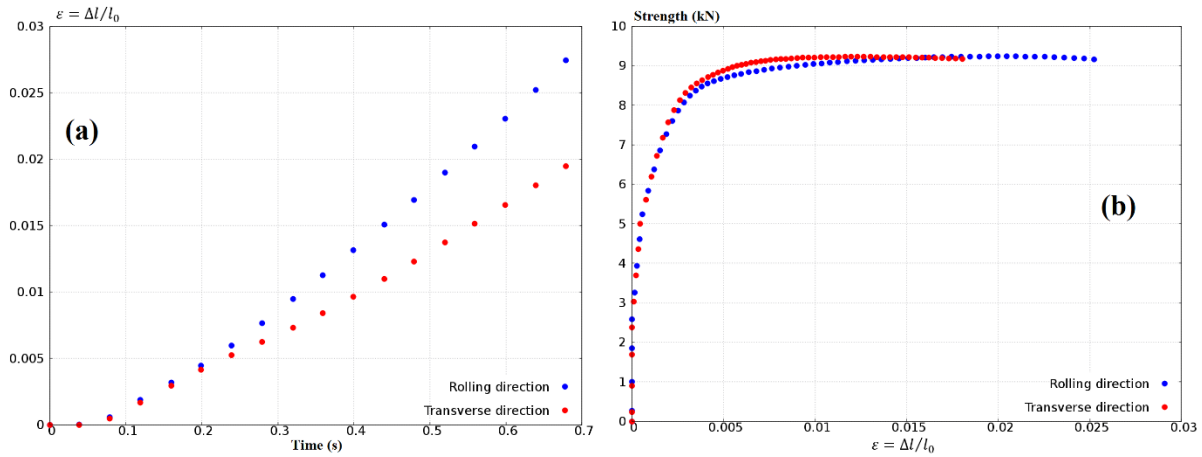


Fig 12. Strain Vs Time (a) – Strength Vs Strain (b)

Strains are measured by DIC method, initial gauge length is  $L_0 = 64$  mm. Fig 12-(a) shows that the strain rate is slightly higher in the rolling direction,  $5 \cdot 10^{-2} \text{ s}^{-1}$  than in the transverse directions  $3.5 \cdot 10^{-2} \text{ s}^{-1}$ . Strains are also measured in the central area of the specimen (0.4 mm of thickness) and we find that the strain rate starts to increase when the deformation is localized in this area.

This first biaxial anisothermal test has gone well, so we expect to carry out other tests with different strain ratios and higher heating rates. Regarding all these complex loadings imposed during the biaxial test, FEM calculation seems to be necessary for better understanding. That will be presented in the next section.

### 3.3 FEM

To correctly simulate numerically complex biaxial anisothermal tests, applied thermo-mechanical loadings should be as close as possible to the real ones. That is possible thanks to temperature and strain field measurements. The temperature field stored by the thermographic infrared camera is imported, as a first step, in Code\_ASTER®. The second step is a projection of the temperature field on a 3D mesh (Fig 13) refined in the central zone where failure is observed.

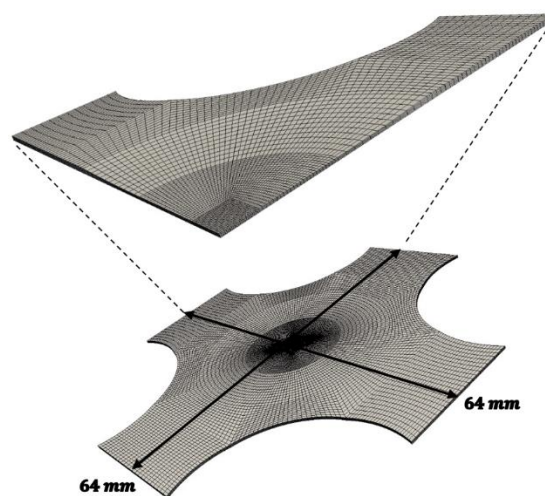


Fig 13. 3D mesh used in FEM

Only half of the thickness is modelled and temperature is assumed homogeneous throughout. An area of 64 mm in both directions which corresponds to the region of interest of the DIC method is modelled. Experimental displacement measured at the four extremities of the

specimen are imposed in the calculations.

Fig 14 shows a comparison between experimental and numerical component of the strain fields along the rolling direction of the specimen. After post-processing the FEM calculations, the same strain localisation is found comparatively to the experimental one. Nevertheless, by comparing experimental and numerical strengths we have found a difference of 20 %. We attribute this difference to a distinct behaviour of plate Zy-4 from cladding Zy-4. In fact, the constitutive law identified on cladding specimens is used for this simulation. The next step in the FEM study should thus consist in identifying a new set of parameters dedicated to the Zircaloy-4 sheet, using tensile isothermal tests performed on the same sheet. Then, the test will be simulated again to evaluate the stress state and calculate stress ratios, and hopefully to assess better the strain distribution.

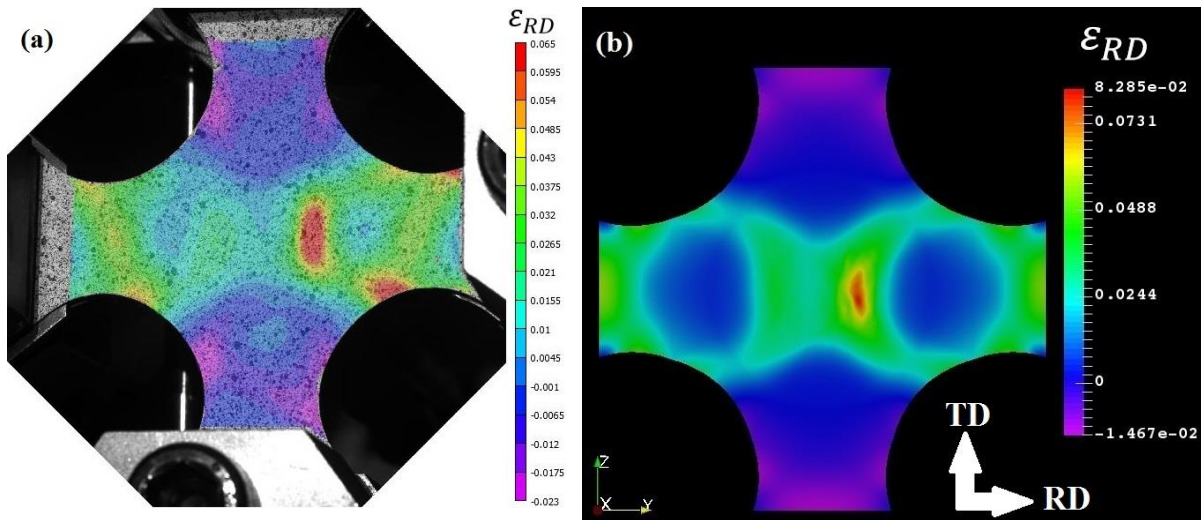


Fig 14. Experimental (a) Vs Numerical (b) strain field in the rolling direction at 560 ms

#### 4. Summary and perspectives

Two experimental devices have been developed to reproduce loadings as close as possible to real RIA loadings on Zircaloy-4 specimens. Tests are carried out at high strain and heating rates, i. e. up to  $5 \text{ s}^{-1}$  and  $560^\circ\text{C}\cdot\text{s}^{-1}$ .

The first uniaxial anisothermal test allows us to assess the history effect on the thermo-mechanical behaviour of clad specimens.

At  $5 \cdot 10^{-1} \text{ s}^{-1}$ , the material showed an important area reduction when the temperature of  $650^\circ\text{C}$  is reached. By analysing mechanical properties, we find that the ultimate stress is higher than the isothermal one especially at high heating rates. We suspect that deviations are due to recrystallization/annealing delays in dependency with the heating rate. Rapid tests carried at  $5 \text{ s}^{-1}$  do not exhibit such features. Anisothermal ultimate stress is similar to that obtained under isothermal conditions. It might be due to the fact that the temperature increase during these tests is limited due to the very fast mechanical loading of the specimens

The FEM simulations of rapid tests show that the material behaviour could be derived from the isothermal tests.

The second developed experimental setup allows us to couple the effects of transient temperature and strain biaxiality. The first test performed has been successful and enables us to move to the next step: the study of the effect of biaxiality ratio on failure during anisothermal tests, with the hope of reaching RIA loadings strain states. Because these tests are quite complex, precise FEM calculations have been undertaken. The modelling will be improved with an updated behaviour model for the thin sheet.

## 5. Acknowledgments

The authors would like to thank operators who have contributed in the experimental test developments. Authors are grateful for their technical support and assistance. This work is funded by EDF through grant P117T.

## 6. References

- [1] J. Desquines, D. A. Koss, A. T. Motta, B. Cazalis and M. Petit, "The issue of stress state during mechanical test to assess cladding performance during reactivity-initiated accident (RIA)," *Journal of Nuclear Materials*, vol. 412, p. 250–267, 2011.
- [2] J. Papin, B. Cazalis, J. Frizonnet, J. Desquines, F. Lemoine, V. Georgenthum, F. Lamare and M. Petit, "Summary and interpretation of the CABRI REP-Na program," *Nuclear Technology*, vol. 157(3), pp. 230-250, 2007.
- [3] F. Schmitz and J. Papin, "High burnup effects on fuel behaviour under accident conditions: the tests CABRI REP-Na," *Journal of Nuclear Materials*, vol. 270, pp. 55-64, 1999.
- [4] T. Fuketa and H. Sasajima, "Behavior of high burnup PWR fuels with low-tin Zircaloy-4 cladding under reactivity-initiated-accident conditions," *Nuclear Technology* 133(1), pp. 50-62, 2001.
- [5] T. Fuketa, F. Nagase, K. Ishijima and T. Fujishiro, "NSRR/RIA experiments with high-burnup PWR fuels," *Nuclear Safety* 37(4), pp. 328-342, 1996.
- [6] B. Cazalis, J. Desquines, C. Poussard, M. Petit, Y. Monerie, C. Bernaudat, P. Yvon and X. Averty, "The PROMETRA program : Fuel cladding mechanical behavior under high strain rate," *Nuclear Technology*, vol. 157, p. 215\_229, 2007.
- [7] A. H. De Menibus, Q. Auzoux, J. Besson and J. Crépin, "Temperature increase of Zircaloy-4 cladding tubes due to plastic heat dissipation during tensile tests at 0.1-10 s<sup>-1</sup> strain rates," *Journal of Nuclear Materials*, Elsevier, 454 (1-3), pp. 247-254, 2014.
- [8] F. Yunchang and D. A. Koss, "The influence of multiaxial states of stress on the hydrogen embrittlement of zirconium alloy sheet," *Metallurgical and Materials Transactions A*, vol. 16, p. 675–681, 1985.
- [9] M. Le Saux, J. Besson, S. Carassou, C. Poussard and X. Averty, "A model to describe the anisotropic viscoplastic mechanical behavior of fresh and irradiated Zircaloy-4 fuel claddings under RIA loading conditions," *Journal of Nuclear Materials*, no. 378, pp. 60-69, 2008.
- [10] M. Le Saux, J. Besson, S. Carassou, C. Poussard and X. Averty, "Behavior and failure of uniformly hydrided Zircaloy-4 fuel claddings between 25 °C and 480 °C under various stress states, including RIA loading conditions," *Engineering Failure Analysis*, vol. 17, no. 3, pp. 683-700, 2010.
- [11] K. Murty and I. Charit, "Texture development and anisotropic deformation of Zircalloys," *Progress in Nuclear Energy* 48, p. 325–359, 2006.
- [12] C. Hunt and E. Schulson, "Recrystallization of Zircaloy-4 during transient heating," *Journal of Nuclear Materials*, vol. 92, pp. 184-190, 1980.
- [13] T. Forgeron, J. C. Brachet, F. Barcelo, A. Castaing, J. Hivroz, J. P. Mardon and C. Bernaudat, "Experimental and Modeling of Advanced Fuel Rod Cladding Behavior Under LOCA Conditions: Alpha-Beta Phase Transformation Kinetics and EDGAR Methodology," *Zirconium in the Nuclear Industry : Twelfth International Symposium*, ASTM STP 1354, G. P. Sabol and G. D. Moan, Eds., American Society for Testing and Materials, West Conshohocken, PA, pp. 256-278, 2000.